Supramolecular motifs and solvatomorphism within the compounds [M(bpy)_3]_2[NbO(C_2O_4)_3]Cl•nH_2O (M=Fe^2+, Co^2+, Ni^2+, Cu^2+ and Zn^2+; n=11, 12). Syntheses, structures and magnetic properties

Jurić, Marijana; Perić, Berislav; Brničević, Nevenka; Planinić, Pavica; Pajić, Damir; Zadro, Krešo; Giester, Gerald; Kaitner, Branko

Source / Izvornik: **Dalton Transactions, 2008, 6, 742 - 754**

Journal article, Accepted version
Rad u časopisu, Završna verzija rukopisa prihvaćena za objavljivanje (postprint)

https://doi.org/10.1039/B707937K

Permanent link / Trajna poveznica: https://urn.nsk.hr/urn:nbn:hr:217:939574

Supramolecular motifs and solvatomorphism within the compounds containing $[M(bpy)_3]^{2+}$ entities: $[M(bpy)_3]_2[NbO(C_2O_4)_3]Cl\cdot nH_2O$ (M = Fe^{2+}, Co^{2+}, Ni^{2+}, Cu^{2+} and Zn^{2+}; bpy = 2,2'-bipyridine; n = 11, 12). Syntheses, structures and magnetic properties

Marijana Jurić,[a] Berislav Perić,*[a] Nevenka Brničević,*[a] Pavica Planinić,*[a] Damir Pajić,[b] Krešo Zadro,[b] Gerald Giester[c] and Branko Kaitner[d]

[a] *Ruđer Bošković Institute, Bijenička cesta 54, 10000 Zagreb, Croatia*
[b] *Department of Physics, Faculty of Science, University of Zagreb, Bijenička cesta 32, 10000 Zagreb, Croatia*
[c] *Institut für Mineralogie und Kristallographie, Universität Wien – Geozentrum, Althanstraße 14, 1090 Wien, Austria*
[d] *Department of Chemistry, Faculty of Science, University of Zagreb, Horvatovac 102a, 10000 Zagreb, Croatia*

Abstract

Solvatomorphism has been found between two series of complexes of the composition $[M(bpy)_3]_2[NbO(C_2O_4)_3]Cl\cdot nH_2O$ [M = Fe^{2+} (**1**, **2**), Co^{2+} (**3**, **4**), Ni^{2+} (**5**, **6**), Cu^{2+} (**7**) and Zn^{2+} (**8**, **9**); bpy = 2,2'-bipyridine)], crystallizing in the monoclinic space group $P2_1/c$ [**3**, **5**, **8** (n = 11)] or in the orthorhombic space group $P2_12_12_1$ [**2**, **4**, **6**, **7** (n = 12)]. All the structures contain two symmetry independent $[M(bpy)_3]^{2+}$ cations, one $[NbO(C_2O_4)_3]^{3-}$ anion, one Cl^- anion, and crystal water molecules. The cations possess a trigonally distorted octahedral geometry, with an additional tetragonal distortion in **7**. Analysis of crystal packing reveals a specific type of supramolecular contact comprising four bipyridine ligands from two neighbouring $[M(bpy)_3]^{2+}$ cations – quadruple aryl embrace (QAE) contact. The contact is realized by the alignment of two molecular two-fold rotation axes, preserving the parallel orientation of the molecular three-fold rotation axes. The resulting two-dimensional honeycomb lattices of $[M(bpy)_3]^{2+}$ cations are placed between the hydrogen bonding layers made of $[NbO(C_2O_4)_3]^{3-}$ and Cl^- anions and the majority of crystal water molecules. The temperature-dependent magnetic susceptibility measurements (1.8–300 K) show a significant orbital angular momentum contribution for **3** and **4** (high-spin Co^{2+}), the influence of zero-field splitting for **5** and **6** (Ni^{2+}) and a substantially paramagnetic Curie behaviour for the Cu^{2+} compound (**7**).

Introduction

Modern ideas in the design of new molecular solids with desirable physical properties, like those used in crystal engineering,[1] are based on the analysis of controlled supramolecular aggregation of molecular entities.[2] Supramolecular aggregates can be well recognized and geometrically characterized using structural data from the X-ray crystallographic methods. Structural data often contain information that is crucial for the understanding of magnetic and other properties of materials. In molecular solids with localized paramagnetic centres, supramolecular aggregates often serve as pathways for the magnetic exchange interactions. Therefore, in research of magnetic materials, it would be useful to classify supramolecular aggregates of paramagnetic centres, according to their suitability for mediation of magnetic exchange interactions.

For a complete understanding of magnetic behaviour of materials, apart from the crystal packing (*i.e.* supramolecular aggregation), it is essential to know the coordination geometry of individual paramagnetic centres. As already documented, deviations from the Curie law of magnetic susceptibilities of transition metal complexes could be the consequence of a combined effect of the ligand-field distortion and spin-orbit interaction.[3–7] These effects are more important for the ions possessing the first-order orbital angular momentum in their ground states, such as the high-spin Fe^{2+} or Co^{2+} ions in the octahedral environment.[3] Additionally, distortions of octahedral ligand field will pronounce the anisotropy of magnetic susceptibility.[8,9]

In the rational synthesis of novel magnetic materials the oxalate anion has appeared as a useful bridging ligand – in constructing a diversity of homo- and heterometallic compounds with attractive new architectures and interesting magnetic properties.[10] As a continuation of our research work on transition metal polynuclear compounds, recently we have synthesized a number of oxalate-bridged transition metal species that exert ferromagnetic exchange interactions within the homodinuclear ($Cu^{II}Cu^{II}$) as well as heterotrinuclear ($Cu^{II}Cr^{III}Cu^{II}$) units,[11,12] by using the anionic tris(oxalate) ligands like $[Cr(C_2O_4)_3]^{3-}$ and $[NbO(C_2O_4)_3]^{3-}$ and various transition metal cations as building blocks.

In this work supramolecular contacts of the $[M(bpy)_3]^{2+}$ entities (M = Fe^{2+}, Co^{2+}, Ni^{2+}, Cu^{2+} and Zn^{2+}) in the solid state of the novel $[M(bpy)_3]_2[NbO(C_2O_4)_3]Cl{\cdot}nH_2O$ (bpy = 2,2'-bipyridine; n = 11, 12) compounds, obtained in the course of the above mentioned investigations, have been described. In general, the best known contact within the crystalline materials involving $[M(bpy)_3]^z$ units (z = 0, +1, +2) is the so-called six-fold aryl embrace

(SAE) realized along the three-fold axes of the molecules.[13] In the present work, the four-fold (quadruple) aryl embrace (QAE), not analysed for the $[M(bpy)_3]$ units in the literature so far, turned out to be predominant. The magnetic behaviour of the title compounds has been studied in view of the suitability of the QAE contacts for the mediation of magnetic exchange interactions. Geometrical distortions of the ligand fields for the individual magnetic centres have also been presented and correlated with the corresponding magnetic measurements.

Experimental

Materials

$M_3[NbO(C_2O_4)_3]\cdot nH_2O$ ($M = NH_4^+$, n = 1; $M = Na^+$, n = 4; $M = Rb^+$, n = 2) and $[M(bpy)_3]Cl_2\cdot nH_2O$ ($M = Co^{2+}$, Ni^{2+} or Cu^{2+}, n = 6; $M = Fe^{2+}$, Zn^{2+}, n = 7; bpy = 2,2'-bipyridine) were prepared according to the literature methods.[14–16] All other reagents used in the syntheses were purchased from commercial sources and applied without further purification. Elemental analyses for C, H and N were carried out using a Perkin Elmer Model 2400 microanalytical analyser. Chlorine was determined by titration with standard 0.04 M $AgNO_3$ solution after decomposition of compounds with KOH and H_2O_2.

Preparations

$[Fe(bpy)_3]_2[NbO(C_2O_4)_3]Cl\cdot nH_2O$ [n = 11 (**1**); n = 12 (**2**)]. To an aqueous solution (10 mL) of $(NH_4)_3[NbO(C_2O_4)_3]\cdot H_2O$ (0.121 g, 0.272 mmol) an aqueous solution (15 mL) of $[Fe(bpy)_3]Cl_2\cdot 7H_2O$ (0.393 g, 0.545 mmol) was added dropwise. The resulting solution remained clear but in a period of 2–3 days a small amount of red precipitate was formed and removed by filtration. Soon after the dark-red needle-like crystals of **1** started to crystallize. The process of crystallization was over in a period of one week, when the mother-liquid was decanted, the crystals were quickly washed by a small amount of water and shortly dried in air. The yield was 0.292g, 64.8%. Found: C, 47.57; H, 4.03; N, 9.98; Cl, 2.20; Calc. for $C_{66}H_{70}N_{12}O_{24}ClNbFe_2$: C, 47.89; H, 4.26; N, 10.15; Cl, 2.14%. IR $\tilde{\nu}$ /cm^{-1}: 3430(m, br), 1713(vs), 1686(vs), 1601(w), 1491(w), 1466(m), 1437(m), 1424(m), 1397(s), 1311(w), 1266(w), 1241(w), 1155(w), 1120(w), 1104(w), 1066(w), 1008(w), 929(w), 900(m), 803(w), 778(vs) 734(m), 657(w), 538(w), 416(w), 420(w).

When the crystals of **1** were left in solution the recrystallization of **1** into polyhedral crystals of **2** took place. The recrystallization process was completed in ~ one month. Then the mother-liquid was decanted, the crystals were quickly washed with water and shortly air-

dried before analysis. The yield was 0.254 g, 55.8%. Found: C, 47.57; H, 4.20; N, 9.81; Cl, 2.16. Calc. for $C_{66}H_{72}N_{12}O_{25}ClNbFe_2$: C, 47.37; H, 4.34; N, 10.04; Cl, 2.12%. IR $\tilde{\nu}$/cm^{-1}: 3430(m, br), 1711(vs), 1684(vs), 1601(m), 1490(w), 1466(m), 1441(m), 1425(m), 1393(s), 1312(w), 1264(w), 1242(w), 1160(w), 1122(w), 1106(w), 1066(w), 1008(w), 930(w), 901(m), 801(w), 777(vs), 734(m), 658(w), 537(w), 416(w), 421(w).

$[Co(bpy)_3]_2[NbO(C_2O_4)_3]Cl\cdot nH_2O$ [n = 11 (**3**); n = 12 (**4**)]. The aqueous solutions of $Na_3[NbO(C_2O_4)_3]\cdot 4H_2O$ (25 mL, 0.202 g, 0.393 mmol) and $[Co(bpy)_3]Cl_2\cdot 6H_2O$ (20 mL, 0.555 g, 0.785 mmol) were mixed as for **1**. The resulting solution soon became cloudy and a yellow precipitate formed together with the yellow-orange single crystals of the composition $[Co(C_2O_4)(bpy)_2]\cdot 5H_2O$.[17] These were separated by filtration and the solution was left to evaporate at ambient conditions. In a two-week period the orange-red single crystals of **3** formed. After two days the crystals of **3**, gathered after the mother-liquid was decanted, were washed and air-dried as for **1**. The yield was 0.193 g, 29.6%. Found: C, 48.02; H, 4.42; N, 10.00; Cl, 2.25. Calc. for $C_{66}H_{70}N_{12}O_{24}ClNbCo_2$: C, 47.71; H, 4.25; N, 10.12; Cl, 2.13%. IR $\tilde{\nu}$/cm^{-1}: 3417(m, br), 1713(vs), 1688(vs), 1596(s), 1491(w), 1472(m), 1442(s), 1393(s), 1313(m), 1262(w), 1248(w), 1178(w), 1161(m), 1127(w), 1103(w), 1063(w), 1018(m), 929(w), 908(m), 802(w), 777(vs), 737(m), 651(w), 631(w), 540(w), 417(w).

The crystals of **3** recrystallize into brown polyhedral single crystals of **4** in a period of 3 weeks, if left in mother-liquid. The yield was 0.165 g, 25.0%. Found: C, 47.01; H, 4.56; N, 9.95; Cl, 2.09. Calc. for $C_{66}H_{72}N_{12}O_{25}ClNbCo_2$: C, 47.20; H, 4.32; N, 10.01; Cl, 2.11%. IR $\tilde{\nu}$/cm^{-1}: 3407(m, br), 1713(vs), 1687(vs), 1597(s), 1492(w), 1473(m), 1442(s), 1394(s), 1314(m), 1263(w), 1249(w), 1177(w), 1161(m), 1127(w), 1103(w), 1064(w), 1018(m), 930(w), 909(m), 802(w), 778(vs), 734(m), 652(w), 632(w), 539(w), 417(w).

$[Ni(bpy)_3]_2[NbO(C_2O_4)_3]Cl\cdot nH_2O$ [n = 11 (**5**); n = 12 (**6**)]. After mixing the aqueous solutions of $Rb_3[Nb(C_2O_4)_3]\cdot 2H_2O$ (8 mL; 0.101 g, 0.152 mmol) and $[Ni(bpy)_3]Cl_2\cdot 6H_2O$ (7 mL; 0.214 g, 0.303 mmol) thin pink-coloured needle-like monoclinic crystals of **5** started to form in 30 minutes. The crystallization was over in 3–4 days. The crystals were separated by filtration, washed with water and air-dried as for **1**. The yield was 0.197 g, 78.2%. Found: C, 47.81; H, 4.21; N, 9.89; Cl, 2.17. Calc. for $C_{66}H_{70}N_{12}O_{24}ClNbNi_2$: C, 47.72; H, 4.25; N, 10.12; Cl, 2.13%. IR $\tilde{\nu}$/cm^{-1}: 3422(m, br), 1718(vs), 1686(vs), 1598(s), 1492(w), 1474(m), 1443(s), 1395(s), 1314(m), 1263(w), 1249(w), 1179(w), 1162(m), 1104(w), 1065(w), 1020(s), 938(w), 908(m), 804(w), 778(vs), 738(m), 653(w), 633(w), 545(w), 419(w).

The crystals of **5**, like those of **1** or **3**, are also metastable in mother-liquid and recrystallize into dark-pink polyhedral single crystals of **6**. This process is completed in a few weeks. The crystals were separated, washed and dried as for **1** or **2**. The yield was 0.182 g, 71.6%. Found: C, 46.95; H, 4.35; N, 9.82; Cl, 2.08. Calc. for $C_{66}H_{72}N_{12}O_{25}ClNbNi_2$: C, 47.21; H, 4.32; N, 10.01; Cl, 2.11%. IR $\tilde{\nu}$ /cm^{-1}: 3403(m, br), 1713(vs), 1686(vs), 1598(s), 1493(w), 1474(m), 1443(s), 1394(s), 1313(m), 1266(w), 1247(w), 1176(w), 1160(m), 1104(w), 1064(w), 1020(s), 931(w), 909(m), 802(w), 778(vs), 738(m), 653(w), 633(w), 541(w), 418(w).

$[Cu(bpy)_3]_2[NbO(C_2O_4)_3]Cl\cdot 12H_2O$ (**7**). The aqueous solutions of $Na_3[NbO(C_2O_4)_3]\cdot 4H_2O$ (10 mL; 0.111 g, 0.216 mmol) and $[Cu(bpy)_3]Cl_2\cdot 6H_2O$ (10 mL; 0.307 g, 0.432 mmol) were mixed as for **1**. From the clear solution, in a three-days period light-blue polyhedral single crystals of the composition $[\{Cu(bpy)_2\}_2(\mu\text{-}C_2O_4)][Cu(bpy)_2(\mu\text{-}C_2O_4)NbO(C_2O_4)_2]_2\cdot 0.5bpy\cdot 7H_2O$ were obtained.[11] In the next two days the dark-blue plate-like single crystals of **7** started to form. The two kinds of single crystals, coexisting in the solution, were separated mechanically. The crystals of **7** were washed and dried as for **1** or **2**. They were stable in the mother-liquid similar to the crystals of **2**, **4** and **6**. The yield was 0.130 g, 35.6%. Found: C, 47.22; H, 4.32; N, 9.89; Cl, 2.28. Calc. for $C_{66}H_{72}N_{12}O_{25}ClNbCu_2$: C, 46.94; H, 4.30; N, 9.95; Cl, 2.10%. IR $\tilde{\nu}$ /cm^{-1}: 3420(m, br), 1725(w), 1711(vs), 1686(vs), 1595(s), 1491(w), 1473(m), 1441(s), 1392(s), 1313(m), 1262(w), 1248(m), 1177(w), 1160(m), 1102(w), 1060(w), 1017(m), 930(w), 909(m), 801(w), 777(vs), 736(m), 652(w), 629(w), 540(w), 417(w).

$[Zn(bpy)_3]_2[NbO(C_2O_4)_3]Cl\cdot nH_2O$ [n = 11 (**8**); n = 12 (**9**)]. After mixing the aqueous solutions of $Na_3[Nb(C_2O_4)_3]\cdot 4H_2O$ (15 mL; 0.109 g, 0.212 mmol) and $[Zn(bpy)_3]Cl_2\cdot 7H_2O$ (15 mL; 0.310 g, 0.424 mmol) the reaction mixture became cloudy. The solution was left for 24 h when a small amount of white precipitate was removed by filtration. Reddish needle-like single crystals of **8** formed in two weeks. They were separated from solution, washed and dried as for **1**. The yield was 0.083 g, 23.4%. Found: C, 47.65; H, 4.16; N, 9.85; Cl, 2.19. Calc. for $C_{66}H_{70}N_{12}O_{24}ClNbZn_2$: C, 47.34; H, 4.21; N, 10.04; Cl, 2.12%. IR $\tilde{\nu}$ /cm^{-1}: 3414(m, br), 1711(vs), 1689(vs), 1595(s), 1491(w), 1474(m), 1441(s), 1388(s), 1314(m), 1262(w), 1249(w), 1178(w), 1160(m), 1104(w), 1063(w), 1017(s), 929(w), 909(m), 800(w), 778(vs), 737(m), 651(w), 630(w), 537(w), 417(w).

The crystals of **8**, similar to those of **1**, **3** and **5**, if left in mother-liquid recrystallized into pink, polyhedral single crystals of **9**. The yield was 0.075 g, 20.8%. Found: C, 47.00; H, 4.26; N, 10.12; Cl, 2.20. Calc. for $C_{66}H_{72}N_{12}O_{25}ClNbZn_2$: C, 46,84; H, 4.29; N, 9.93; Cl, 2.09%. IR $\tilde{\nu}$ /cm^{-1}: 3424(m, br), 1712(vs), 1689(vs), 1595(s), 1491(w), 1474(m), 1442(s), 1389(s), 1314(m), 1261(w), 1249(w), 1178(w), 1160(m), 1103(w), 1064(w), 1017(s), 929(w), 909(m), 800(w), 778(vs), 737(m), 652(w), 630(w), 538(w), 417(w).

Physical measurements

Infrared spectra were recorded as KBr pellets on an ABB Bomem FT model MB 102 spectrometer in the 4000–200 cm^{-1} region.

The magnetic data for compounds **3**–**7** were collected on a commercial SQUID magnetometer (MPMS-5, Quantum Design). The measurements were performed in the temperature range 1.8–290 K for the applied magnetic field of 1 T for **3** and **4** and 0.01 T for **5**, **6** and **7**. The field dependence of the magnetic moments for **3** and **4** was checked up to 5 T and the compounds showed linearity up to more than 1 T. Prior to any calculation, the measured data were corrected against the sample holder's contribution. Diamagnetic corrections for the constituent atoms were estimated from the Pascal's constants.[18] For the determination of the model parameters from the magnetic susceptibility measurements with nonlinear fit procedures, the software system "Mathematica" was used.[19]

X-Ray crystallography

Single crystals of compounds **1** and **9** were not of quality needed for the X-ray analysis. Suitable single crystals of **2**–**6** and **8** were selected and mounted on an Enraf-Nonius KappaCCD diffractometer, equipped with a monocapillary optics collimator, whereas for **7** a four-circle Philips PW1100 diffractometer (updated by Stoe) was used. All data were obtained by graphite monochromated Mo-Kα radiation (λ = 0.71073 Å) at 200 K, except for **7** that was measured at room temperature. Crystals of **3**, **5** and **8** were of needle form with one dimension larger than other two (0.3 × 0.05 × 0.05 mm), whereas crystals of **2**, **4**, **6** and **7** were of rhombohedral form (0.12 × 0.1 × 0.1 mm) and chosen small enough to avoid the errors generated by the absorption of X-rays in the samples. Unit cell parameters for **2**–**6** and **8** were determined based on all collected data using the DENZO-SCALEPACK program,[20] whereas for **7** these parameters were obtained from 45 reflections collected in the θ range of 10.2–15.4^o, with the STADI4 program.[21] The Lorentz-polarization correction for **7** was performed by the X-RED program,[22] for other compounds the DENZO-SCALEPACK program[20] was

used. By using this program during the scaling of the reflection intensities, the multi-scan absorption correction and correction for decay of the samples was already included,[23] whereas for compound **7** the decay correction (10.9%) was made using the X-RED program.[22] The details of the crystallographic structural analyses are summarized in Table 1. All the structures were solved by the SHELXS-97 program[24] and refined by the SHELXL-97 program.[25] In order to test the isostructurality among the orthorhombic compounds, the best structure solution in this series [**2**, R_1 = 0.0411] was used as a starting model in the refinement of the rest of the orthorhombic structures (**4**, **6** and **7**). All atoms in these structures retained reasonable atomic displacement parameters. A similar procedure was applied in the refinement of the monoclinic compounds. The structural solution of the best quality [**8**, R_1 = 0.0408] was used as a starting model in the refinement of the rest of the monoclinic structures (**3** and **5**). During the refinement of **3**, it was observed that the atomic displacement parameters of Cl^- anion were unusually large, while the same parameters for two crystal water molecules [O(19) and O(21)] were unusually small. It was assumed that these three constituents occupy their positions disorderly. Occupancies of these positions were refined in subsequent least-squares refinement cycles. Also, the crystal water molecules O(16) and O(21) of **3** showed an unusual elongation of the atomic displacement parameters. Consequently, the disorder of these atoms was taken into account: the O(16) atom was given two positions, O(161) and O(162), with the probability of 40 and 60%, respectively; the O(21) atom was given two positions, O(211) and O(212), of equal probability. The hydrogen atoms attached to carbon atoms in all the compounds were treated as riding, with the C−H distances of 0.93 Å and U_{iso} (H) = 1.2U_{eq}(C). Their positions were generated using the SHELXL-97 program.[25] The structural solutions of the best quality (**8** and **2**) were analyzed by further difference Fourier syntheses, where some peaks were recognized as hydrogen atoms of crystal water molecules. The remaining hydrogen atoms were determined using the M. Nardelli algorithm[26] implemented in the WINGX program.[27] All hydrogen atoms had plausible hydrogen bonding interpretation and in the final least-squares refinement procedures the ideal geometry restraints (the O−H distance of 0.84 Å and H−O−H angle of 104^o) were applied. The only exception from this procedure was the structural refinement of **3**, where the positions of hydrogen atoms from the crystal water molecules were not determined at all, due to the observed occupancy disorder of Cl^- anion and several crystal water molecules.

CCDC reference numbers 648552–648558.

See http://www.rsc.org/suppdata/dt/xy/xyz for crystallographic data in CIF or other electronic format.

Table 1 Crystallographic data for compounds **2**–**8**

Compound* (M)	**2** (Fe)	**3** (Co)	**4** (Co)	**5** (Ni)	**6** (Ni)	**7** (Cu)	**8** (Zn)
M/g mol^{-1}	1673.42	1661.56	1679.58	1661.08	1679.10	1688.82	1674.48
Crystal system	Orthorhombic	Monoclinic	Orthorhombic	Monoclinic	Orthorhombic	Orthorhombic	Monoclinic
Space group	$P2_12_12_1$	$P2_1/c$	$P2_12_12_1$	$P2_1/c$	$P2_12_12_1$	$P2_12_12_1$	$P2_1/c$
a/Å	14.975(1)	23.548(3)	15.103(1)	23.875(3)	15.058(1)	15.035(1)	24.070(2)
b/Å	21.708(2)	13.631(1)	22.075(2)	13.265(1)	22.039(2)	22.267(2)	13.332(1)
c/Å	22.351(2)	22.812(2)	22.386(3)	23.115(2)	22.398(2)	22.538(3)	23.168(2)
α/^{o}	90	90	90	90	90	90	90
β/^{o}	90	101.04(1)	90	101.69(1)	90	90	102.19(1)
γ/^{o}	90	90	90	90	90	90	90
V/Å^3	7266(1)	7187(1)	7463(1)	7169(1)	7433(1)	7545(1)	7267(1)
Z	4	4	4	4	4	4	4
D_c/g cm^{-3}	1.530	1.536	1.495	1.539	1.500	1.487	1.531
μ/cm^{-1}	0.674	0.753	0.712	0.802	0.775	0.828	0.933
F(0,0,0)	3448	3416	3456	3424	3464	3472	3440
Θ_{max}/^{o}	30.53	28.31	30.51	30.55	30.49	27.05	30.52
Unique reflections	22167	17763	22725	21837	22608	16364	22113
Observed reflections	15502	12012	16932	10419	16952	9976	14954
R_{int}	0.0323	0.0354	0.0388	0.1067	0.0344	0.0358	0.0336
No. of parameters	1036	976	1033	1033	1033	1024	1033
R_1 ($I > 2\sigma(I)$), wR_2	0.0411, 0.0937	0.0500, 0.1314	0.0507, 0.1219	0.0627, 0.1367	0.0461, 0.1270	0.0538, 0.1457	0.0408, 0.1068
Flack param., conf.[28]	–0.013(8), δ		–0.02(1), δ		0.004(9), δ	0.00(1), λ	
Goodness of fit	0.993	1.032	1.015	0.965	1.037	1.009	1.025
$\Delta\rho_{max}$, $\Delta\rho_{min}$	0.843, –0.400	1.304, –0.558	1.311, –0.823	1.428, –1.129	1.487, –0.766	0.850, –0.544	1.770, –0.764

*Chemical formula: $[M(bpy)_3]_2[NbO(C_2O_4)_3]Cl\cdot 11H_2O$ (**3**, **5** and **8**) or $[M(bpy)_3]_2[NbO(C_2O_4)_3]Cl\cdot 12H_2O$ (**2**, **4**, **6** and **7**)

Results and discussion

The new complex salts of the formulae $[M(bpy)_3]_2[NbO(C_2O_4)_3]Cl\cdot nH_2O$ (M = Fe^{2+}, Co^{2+}, Ni^{2+}, Cu^{2+} and Zn^{2+}; n = 11, 12) resulted from the reactions of $[M(bpy)_3]^{2+}$ and $[NbO(C_2O_4)_3]^{3-}$ performed in aqueous solutions in the molar ratios of 2 : 1. The compounds formed also when the starting components were mixed in the ratios of 1 : 1 and 3 : 2, but the yields of the reactions were somewhat lower.

The metastable, obviously thermodynamically less favoured, needle-like monoclinic crystals $[M(bpy)_3]_2[NbO(C_2O_4)_3]Cl\cdot 11H_2O$ (M = Fe^{2+}, Co^{2+}, Ni^{2+} and Zn^{2+}) formed first, which, if left in solution, slowly transformed into the more stable orthorhombic compounds crystallizing with one more crystal water molecule. For copper(II) only the orthorhombic complex was obtained, which co-crystallized in solution with the previously reported $[\{Cu(bpy)_2\}_2(\mu\text{-}C_2O_4)][Cu(bpy)_2(\mu\text{-}C_2O_4)NbO(C_2O_4)_2]_2\cdot 0.5bpy\cdot 7H_2O$.[11] The complexes obtained are rather insoluble in water and common organic solvents.

Molecular structures and distortions of $[M(bpy)_3]^{2+}$ cations

All the structures contain two symmetry independent $[M(bpy)_3]^{2+}$ cations (**A** and **B**), one $[NbO(C_2O_4)_3]^{3-}$ anion and one Cl^- anion, together with 11 or 12 crystal water molecules for the monoclinic and orthorhombic compounds, respectively. Fig. 1 shows ORTEP-3[29] drawings of the **A** and **B** cations of one orthorhombic [M = Fe (**2**); Fig. 1a] and one monoclinic [M = Zn (**8**); Fig. 1b] compound as well as of the $[NbO(C_2O_4)_3]^{3-}$ anion (from the structure of **2**, Fig. 1c), with the atomic numbering schemes. It can be seen that the mutual orientation of the two symmetry independent cations in two different crystallographic forms is similar. There is no significant difference in the conformation of the $[NbO(C_2O_4)_3]^{3-}$ anion among the structures, either. The conformation is practically the same as that found in $Rb_3[NbO(C_2O_4)_3]\cdot 2H_2O$ or $(NH_4)_3[NbO(C_2O_4)_3]\cdot H_2O$.[14,15] Within the distorted pentagonal-bipyramidal coordination polyhedra around niobium the interatomic distances for all species fall into the ranges 1.714(2)–1.722(2) and 2.093(2)–2.212(2) Å for the Nb=O and Nb−O bonds, respectively. The bond-valence analysis applied to the appropriate bond lengths leads to a diamagnetic (+5) oxidation state of Nb atoms.[30]

Metal atoms in the $[M(bpy)_3]^{2+}$ cations are octahedrally coordinated by six N atoms. The interatomic M−N distances are in the following ranges: 1.965(2)–1.981(2) Å for Fe^{2+} cations, 2.102(3)–2.138(3) Å for Co^{2+} cations, 2.066(3)–2.103(3) Å for Ni^{2+} cations, 2.042(5)–2.243(5) Å for Cu^{2+} cations and 2.136(2)–2.182(2) Å for Zn^{2+} cations. The Fe−N distances in **2** do not exceed 2 Å, as typical for the low-spin Fe^{2+} species,[31] as distinct from the high-spin

Fe^{2+} complexes usually having Fe−N values of ~ 2.2 Å.[3,32] Also, the Co−N distances in **3** and **4** are typical for the high-spin Co^{2+} species (~ 2.12 Å); the corresponding values for the low-spin Co^{2+} complexes should be shorter by ~ 0.1 Å.[32] Metal atoms are, in all structures, located at the general crystallographic positions. Therefore, their octahedral environments can be distorted in a general way. In the present case the trigonal distortion should be the most prominent – due to the rigidity of the didendate bipyridine-ligand molecules. These ligands will couple six nitrogen atoms into three pairs, displacing them from an ideal octahedral position. Therefore, the $[M(bpy)_3]^{2+}$ cations should be described in the D_3 molecular symmetry group.[33] The trigonal distortion can be assessed by the N−M−N bite angles, *i.e.* by the *cis* N−M−N angles with the N atoms coming from the same ligand molecule. Their values are in the range 75.6(2)–81.72(9)°. The other *cis* N−M−N angles (*i.e.* those with the N atoms from two different bpy molecules) are in the range 89.3(1)–98.7(2)°. The interatomic M−N distances should not be affected by the trigonal distortion, because all six nitrogen atoms can retain mutual symmetry equivalence in the point group D_3. Trigonal distortion can be described by the degree of compression (ratio *s*/*h*) and the angle of twisting ϕ (Fig. 2). The value of *h* represents a distance between the centres of gravity of the two particular triangles, these being [N(1), N(3), N(5)] and [N(2), N(4), N(6)] for the **A** cations, and [N(7), N(9), N(11)] and [N(8), N(10), N(12)] for the **B** cations. The value of *s* corresponds to the average N···N distance inside the corresponding pair of triangles. By projecting the [N(2), N(4), N(6)] and [N(8), N(10), N(12)] triangles to the planes defined by the [N(1), N(3), N(5)] and [N(7), N(9), N(11)] triangles, respectively, it becomes possible to structurally determine the ϕ angles as the average values of the N−M−N angles inside the hexagons obtained by the projections. The values obtained of *s*/*h* and ϕ for both **A** and **B** cations in compounds **2**–**8** are listed in Table 2. The data show that the cations are compressed and twisted, $s/h > 1.22$ and $\phi < 60^o$ (1.22 and 60° are the values for a perfect octahedron).[34] Therefore, the crystallographic data undoubtedly show a trigonal structural distortion of $[M(bpy)_3]^{2+}$ cations in all compounds investigated.

The tetragonal distortion of an octahedron ($O_h \rightarrow D_{4h}$) should be recognized by the differences in the M−N distances. From the above mentioned ranges for these distances it is evident that for compounds **2**–**6** and **8** (including both types of cations), the fluctuation is not larger than 0.05 Å, showing that the tetragonal distortion is very small. However, in the **B** cation of **7** (Cu^{2+} ion) the two *trans* bonds Cu(2)−N(8) and Cu(2)−N(11) [with the values of 2.205(5) and 2.243(5) Å, respectively; ligand numbering as in Fig. 1a] are significantly larger than the other four [2.057(5)–2.085(5) Å], thus indicating a tetragonal elongation in the

direction of the two noted bonds. In the **A** cation of the same compound, the two longest bond lengths are also oppositely oriented: Cu(1)−N(2) and Cu(1)−N(5) [having the values of 2.181(5) and 2.186(5) Å, respectively] as well as the two shortest bond lengths: Cu(1)−N(1) and Cu(1)−N(4) [with the values of 2.060(4) and 2.042(5) Å, respectively]. The fluctuation of the Cu−N distances in the **A** cation of **7** is 0.144 Å, *i.e.* almost three times larger than fluctuations in the other compounds, so a tetragonal distortion is present in the **A** cations of **7**, as well. Tetragonal distortion of coordination octahedra of Cu^{2+} ions is usually attributed to the Jahn-Teller effect, the natural tendency of the complexes with orbitally degenerate ground states to transform themselves spontaneously into energetically more favourable distorted conformations without orbital degeneration.[35] The ground state of Cu^{2+} ion in an octahedral environment is orbitally two-fold degenerate E_g state.[35] The tetragonal distortion ($O_h \rightarrow D_{4h}$) splits this state into two orbitally nondegenerate states: A_{1g} and B_{1g}.[35,36] It is interesting that the trigonal distortion $O_h \rightarrow D_3$ does not remove the orbital degeneracy of the ground state ($E_g \rightarrow E$).[36]

The bpy molecules are almost planar, but some of them are slightly twisted along the C−C bond connecting two pyridyl rings. The largest distortions are found in the **B** cations of the monoclinic compounds [12.4(2)^o for bpy(5) in **3**, 11.1(2)^o for bpy(5) in **5** and 10.6^o for bpy(6) in **8**].

Table 2 Trigonal distortion parameters for the $[M(bpy)_3]^{2+}$ cations in compounds **2**–**8** and inclination of their three-fold axes to the crystallographic direction *c** (*i*)

Compound (M)	**2** (Fe)		**3** (Co)		**4** (Co)		**5** (Ni)		**6** (Ni)		**7** (Cu)		**8** (Zn)	
unit	**A**	**B**	**A**	**B**	**A**	**B**	**A**	**B**	**A**	**B**	**A**	**B**	**A**	**B**
s/*h*	1.35(2)	1.36(2)	1.44(3)	1.42(3)	1.42(4)	1.43(3)	1.39(3)	1.40(4)	1.39(3)	1.39(3)	1.40(4)	1.42(8)	1.40(3)	1.41(6)
ϕ (°)	51.8(6)	51.5(6)	48.2(5)	47.9(7)	47.4(9)	48.0(7)	48.4(5)	50(1)	48.4(7)	49.0(6)	47.0(8)	47(2)	45.2(7)	47(1)
i (°)	6.35(1)	4.83(1)	1.49(2)	6.86(2)	5.99(2)	2.98(2)	1.87(2)	3.60(2)	6.00(2)	3.25(2)	6.3(3)	3.5(3)	2.70(1)	3.64(1)

Description of the crystal structures

The constituent structural units: $[M(bpy)_3]^{2+}$ cations, $[NbO(C_2O_4)_3]^{3-}$ and Cl^- anions and crystal water molecules, are arranged in two different crystal packing forms (orthorhombic and monoclinic) which are represented by stereodrawings in Fig. 3. It is evident that both forms exhibit a layered type of packing: the layers of $[M(bpy)_3]^{2+}$ cations are located between the layers consisting of $[NbO(C_2O_4)_3]^{3-}$ and Cl^- anions and majority of crystal water molecules. All layers are parallel with the *ab* planes of the unit cells. It is interesting that the monoclinic form is a racemic structure containing equal number of different $[M(bpy)_3]^{2+}$ enantiomers (δ and λ), whereas the orthorhombic form is an enantiopure structure containing only one type of $[M(bpy)_3]^{2+}$ enantiomers (δ or λ, Table 1). This is related with a centrosymmetric character of the space group $P2_1/c$ of the monoclinic structures, with respect to the non-centrosymmetric character of the space group $P2_12_12_1$ of the orthorhombic structures. Thus, transformation of the monoclinic crystals into the more stable orthorhombic form during crystallization (see "Experimental") is in fact a process of spontaneous resolution[37] of the racemic compounds $[M(bpy)_3]_2[NbO(C_2O_4)_3]Cl\cdot 11H_2O$ ($M = Fe^{2+}$, Co^{2+}, Ni^{2+}, Zn^{2+}) into the racemic conglomerates $[M(bpy)_3]_2[NbO(C_2O_4)_3]Cl\cdot 12H_2O$. The two structural forms differ in composition just in the number of solvate (water) molecules (11 *versus* 12); therefore, this series of compounds exhibits at the same time the phenomenon of solvatomorphism.[38] Within the monoclinic and orthorhombic forms the complexes are isostructural with the low unit cell similarity indices[39] (0.013 and 0.009 for the monoclinic structural pairs **3**/**5** and **3**/**8**, respectively; 0.009, 0.008 and 0.014 for the orthorhombic structural pairs **2**/**4**, **2**/**6** and **2**/**7**, respectively).

Packings of the $[M(bpy)_3]^{2+}$ cations in one layer for the orthorhombic and monoclinic structures are shown in Figs. 4 and 5, respectively. It is evident that each symmetry independent cation (**A** or **B**) is surrounded by three neighbouring cations; each **A** cation is surrounded by 2 other **A** and one **B** cation, whereas each **B** cation is surrounded by 2 other **B** and one **A** cation. Each neighbouring pair forms a specific supramolecular contact involving four bipyridine ligands, two from one cation and two from the other. By way of example, the neighbouring pair of symmetry independent cations **A** and **B** (Figs. 1, 4 and 5) are in contact through the following bpy ligands: bpy(1)(**A**)···bpy(5)(**B**) and bpy(2)(**A**)···bpy(4)(**B**). This kind of contact has been termed as quadruple aryl embrace – QAE, after Dance and Scudder[13a], who originally termed a similar supramolecular pattern as OQAE (orthogonal quadruple aryl embrace). In our analyses we did not find any evidence of the C–H···π

interactions between the aryl rings which would prefer mutual orthogonal orientation of the bpy ligands. We did not observe any stacking interactions either, concluding that the orientation of the ligands is specific for this kind of supramolecular contacts. For these reasons, the QAE contact between the symmetry independent $[M(bpy)_3]^{2+}$ cations **A** and **B** [QAE(I)], as well as the other two symmetry independent QAE contacts encountered in both structural forms [QAE(II) and QAE(III), Figs. 4 and 5] are described by the distances between the centres of gravity of the entire bpy ligands which are in short contacts [*i.e.* bpy(I)···bpy(II') and bpy(II)···bpy(I'), Table 3] and by the angles between the normals to their least-squares planes (*i.e.* ⊄[bpy(I), bpy(II')] and ⊄[bpy(II), bpy(I')], Table 3). The distances between metal atoms of two connected $[M(bpy)_3]^{2+}$ cations are also given in Table 3. The resulting architecture is consistent with a two-dimensional honeycomb lattice, although the differences in the three crystallographic independent QAE contacts distort the ideal hexagonal symmetry of the lattice. The similarity of packing arrangement of $[M(bpy)_3]^{2+}$ cations in the two types of structures leads to a conclusion that the two structural forms can be considered as homeostructural groups.[40]

A common feature of all QAE contacts encountered in the compounds investigated is that they are aligned in the direction of the local, non-crystallographic C_2 axes of the individual $[M(bpy)_3]^{2+}$ cations. For instance, in the QAE(I) contact shown in Fig. 4, a local (approximate) C_2 axis of the **A** cation, passing through the middle of the ligand bpy(3) and through the metal atom, is in the line with the local C_2 axis of the **B** cation, passing through the middle of the ligand bpy(6) and through the metal atom. The **A** and **B** cations can be mutually related by an additional approximate C_2 symmetry with an axis parallel to the local C_3 axes of both cations and passing through the middle of the line connecting the two metal atoms. In comparison with the well described SAE (sextuple aryl embrace) contact,[13a] several conclusions can be made on the QAE contact, as another type of supramolecular aggregation of two $[M(bpy)_3]$ units in the solid state:

(i) the $[M(bpy)_3]$ units in the QAE contact are homochiral because they can be related with the proper C_2 symmetry. Contrarily, two $[M(bpy)_3]$ units in the SAE contact are of opposite chirality (related through the centre of inversion);[13a]

(ii) the QAE contact is realized along the C_2 symmetry axes of $[M(bpy)_3]$ units. As there are three equivalent C_2 axes in the D_3 symmetry group (lying in the plane and forming mutual angles of 120^o), the QAE contacts will induce the formation of two-dimensional honeycomb lattices in the solid state. The SAE contacts are realized along the C_3 symmetry axes of

$[M(bpy)_3]$ units, so formation of one-dimensional chains of $[M(bpy)_3]$ units in the solid state is preferred;[13a]

(iii) a common feature of both types of contacts is the parallel orientation of the molecular C_3 axes of two aggregated $[M(bpy)_3]$ units.

The honeycomb hexagonal lattices formed by the QAE contacts appear to be a common structural motifs of $[M(bpy)_3]$ units (M = transition metal) in the solid state. The search of the Cambridge Crystallographic Database[41] showed that 34 out of 153 different crystal structures containing neutral or charged $[M(bpy)_3]$ entities (with 3D data) possess honeycomb lattices created by the QAE contacts similar to these described in the present work. Also, in the additional 15 structures one-dimensional zig-zag motifs are formed with the neighbouring $[M(bpy)_3]$ units connected *via* the QAE contacts. Thus, the QAE contacts seem to be more frequent than the SAE ones (21 hits in the search).

In the structures of the compounds investigated, the C_3 and C_2 axes of individual $[M(bpy)_3]^{2+}$ cations as well as the additional C_2 axes relating two neighbouring pairs of cations, are only approximate. If these symmetries were exact, the distances bpy(I)···bpy(II') and bpy(II)···bpy(I') as well as the angles ⊄[bpy(I), bpy(II')] and ([bpy(II), bpy(I')] should be identical. Also, the alignments of molecular C_2 axes into one line, during the formation of a QAE contact, are also approximate. Therefore, the values for characteristic distances and angles (Table 3) deviate among each other. From the data in Table 3, the largest deviations show the QAE(III) contacts of the monoclinic compounds. Remarkably, these contacts involve exactly the most twisted bpy ligands in the structures (see "Molecular structures and distortions of $[M(bpy)_3]^{2+}$ cations"). The relative orientation of four bpy ligands inside one QAE contact is to a great extent determined by the approximate C_2 symmetry relating two aggregated $[M(bpy)_3]$ units. In such a way only the C–H groups from the positions 4, 5, 6, 4', 5' or 6' come close to each other (numbers represent standard numeration of the atomic positions in the bipyridine molecule). Several short intermolecular C···C and C···H contacts were observed in the crystal structures of the investigated compounds, but they are all larger than 3.28 Å (for the C···C contacts) and 2.82 Å (for the C···H contacts). These long intramolecular contacts and canted orientation of the bpy ligands suggest that the QAE contacts are not favourable structural motifs for the mediation of magnetic exchange interactions. The formation of the honeycomb two-dimensional lattice with parallel orientation of the three-fold rotation axes of $[M(bpy)_3]^{2+}$ cations could have significant influence on anisotropic properties of the investigated compounds. All three-fold axes tend to be parallel with the c^* crystallographic directions, *i.e.* orthogonal with the *ab* planes of the

unit cells. As the QAE contacts in the investigated structures are found to be distorted, the local three-fold axes of $[M(bpy)_3]^{2+}$ cations are not completely aligned in the *c** directions, but show a small inclination (*i*). These inclinations have been measured for each type of $[M(bpy)_3]^{2+}$ cations in the crystal structures investigated and the results are listed in Table 2. It was assumed that the local three-fold rotation axes pass through the centres of gravity of the appropriate triangles of the coordinated nitrogen atoms (these are defined in the section "Molecular structures and distortions of $[M(bpy)_3]^{2+}$ cations"). It is evident that the inclinations never exceed 7^o. Assuming that the trigonal distortions of the ligand field environments of individual metal atoms are the most prominent structural distortions, it can be concluded that the both structural types should exhibit an anisotropic behaviour of the physical quantities that can be described as the second-rank tensors (*i.e.* magnetic susceptibility, *g*-value) with one principal axis roughly oriented in the *c** crystallographic directions. As previously mentioned, the cations in the structure of **7** show an additional tetragonal distortion in the direction of the elongated Cu−N bonds, so the principal directions of anisotropic physical quantities in this compound should be more inclined with respect to the *c** crystallographic directions.

Regarding chiralities of $[M(bpy)_3]^{2+}$ cations in all the structures investigated, it is evident that the cations belonging to one honeycomb layer are homochiral, because all of them are connected *via* the QAE contacts which preserve chiralities. Even, in the centrosymmetric monoclinic form, a segregation of the cations into homochiral layers occurs. Thus, in this form the neighbouring layers are of opposite chirality, due to the centres of inversion located between them. On the other hand, the orthorhombic form as a whole exhibits homochirality, as the neighbouring layers are related with the proper two-fold screw symmetry.

Table 3 Structural parameters for QAE contacts

Comp.	bpy(I)···bpy(II') (Å)	bpy(II)···bpy(I') (Å)	⊄[bpy(I), bpy(II')] (°)	⊄[bpy(II), bpy(I')] (°)	M···M (Å)
QAE(I) bpy(I) = bpy(1); bpy(II') = bpy(5); bpy(II) = bpy(2); bpy(I') = bpy(4)					
2	4.88	5.09	50.52	46.34	7.47
3	4.91	5.69	60.30	50.10	8.15
4	4.77	5.00	50.90	43.80	7.54
5	5.06	5.89	66.60	50.20	8.36
6	4.81	5.06	50.99	44.66	7.55
7	4.85	5.01	51.30	44.50	7.57
8	5.03	5.92	67.36	51.36	8.47
QAE(II) bpy(I) = bpy(2); bpy(II') = bpy(3)^{i}; bpy(II) = bpy(3); bpy(I') = bpy(1)^{i}					
2	5.44	5.68	56.35	46.45	8.23
3	4.96	5.12	55.40	48.52	7.86
4	5.30	5.66	57.80	46.50	8.34
5	4.91	4.89	53.04	49.88	7.66
6	5.34	5.68	57.18	46.62	8.31
7	5.30	5.67	56.80	47.40	8.34
8	4.85	4.86	52.32	50.71	7.70
QAE(III) bpy(I) = bpy(6) ; bpy(II') = bpy(5)^{ii}; bpy(II) = bpy(4); bpy(I') = bpy(6)^{ii}					
2	5.82	5.54	45.15	57.97	8.30
3	6.01	4.60	35.20	52.20	7.81
4	5.83	5.42	44.40	60.10	8.42
5	6.12	4.53	29.20	51.80	7.72
6	5.82	5.45	44.60	59.40	8.38
7	5.87	5.40	43.70	60.30	8.42
8	6.11	4.46	29.52	49.92	7.72

Symmetry codes: (i) 1/2 + *x*, 1/2 – *y*, –*z*; (ii) 1/2 + *x*, 3/2 – *y*, –*z* for **2**, **4** and **6**;
(i) –1/2 + *x*, 3/2 – *y*, 2 – *z*; (ii) –1/2 + *x*, 1/2 – *y*, 2 – *z* for **7** and
(i) –*x*, 1/2 + *y*, 1/2 – *z*; (ii) 1 – *x*, 1/2 + *y*, 1/2 – *z* for **3**, **5** and **8**

Hydrogen bonds

In both, the orthorhombic and monoclinic structural forms, two-dimensional honeycomb lattices of $[M(bpy)_3]^{2+}$ cations are positioned between the hydrogen bonding layers made of $[NbO(C_2O_4)_3]^{3-}$ and Cl^- anions and of the majority of crystal water molecules. Main features of the hydrogen bonds for the orthorhombic (**2**) and the monoclinic (**8**) forms are shown in Figs. 6a and 6b, respectively (hydrogen bond parameters are deposited in the supplementary CIF file). Several hydrogen bonds have an important role in connecting two-dimensional layers into a final three-dimensional skeletons, like those involving one water molecule [O(25)] in the orthorhombic form (Fig. 6a) and those involving two water molecules [O(23) and O(24)] in the monoclinic form (Fig. 6b). Hydrogen bonds in the orthorhombic structures are realized without any kind of structural disorder. In the structures of the monoclinic form, some crystal water molecules are located in the vicinities of the crystallographic centres of inversion inducing positional disorder of some of hydrogen atoms attached to them. Nevertheless, each hydrogen atom from any crystal water molecule still participates in some kind of hydrogen bond as in the case of the orthorhombic form.

Stability of the orthorhombic and monoclinic forms

During the preparation of the samples, it was observed that the single crystals of the monoclinic form transform themselves into the crystals of orthorhombic form, if left long enough in mother liquor (see "Experimental" section). This observation leads to the conclusion that the orthorhombic form is energetically the more stable structural type. Structural analysis shows at least three arguments in support of this conclusion: (i) in the packing of the $[M(bpy)_3]^{2+}$ cations it was shown that the most distorted QAE contacts and also the most twisted bpy ligands were observed in the monoclinic structures; (ii) the analysis of hydrogen bonding networks in the monoclinic structures shows disorder of several hydrogen atoms. On the contrary, in the orthorhombic structures all hydrogen atoms from the crystal water molecules are arranged in a hydrogen bonding skeleton without disorder; (iii) some of the distances between the anions in the hydrogen bonding layers of the monoclinic crystal forms are shorter than analogous distances in orthorhombic structures. For example, the shortest Cl···Nb distance (the distance between the Cl^- and $[NbO(C_2O_4)_3]^{3-}$ anions) in the monoclinic form is 6.6085(15) Å; the shortest Cl···Nb distance in the orthorhombic form is 7.4003(11) Å. The distances between two nearest neighbouring Cl^- anions in the monoclinic form are 7.0858(19) and 7.6380(19) Å, whereas in the orthorhombic form there is no distance

between neighbouring Cl^- anions shorter than 10 Å. Therefore, ionic repulsions between anions in hydrogen bonding layers in the monoclinic form should be greater than analogous repulsions in the orthorhombic form.

Infrared spectra

The spectra of complexes **1**–**9** show the absorption bands that can, in general, be attributed to the presence of bipyridine ligand, didentate oxalate groups, oxo-oxygen atom (Nb=O) and crystal water molecules. The positions of the absorption maxima for one pair of solvatomorphs (*i.e.* for a monoclinic and an orthorhombic compound of the same metal ion) are almost identical, and only small differences could be noticed between the spectra of different pairs of solvatomorphs. Two strong, relatively close, absorption bands with maxima at 1711 and 1684 cm^{-1} [ν_{as}(CO)], a strong absorption band at 1393 cm^{-1} and a medium one at 1264 cm^{-1} [ν_s(CO)], together with a band of medium intensity at 801 cm^{-1} [δ(OCO)] (quoted for complex **2**) support the presence of didentate (chelating) oxalate groups – as confirmed by the X-ray diffraction analysis. In the spectra of all complexes a medium intensity absorption at ~ 930 cm^{-1} indicates the presence of the Nb=O bond. The other absorption bands in the spectra originate from the vibrations of coordinated bpy ligand and crystal water molecules.

Magnetic properties

The measurements for compounds **1** and **2** that contain $[Fe(bpy)_3]^{2+}$ cation, showed a very low signal on SQUID magnetometer, supporting the diamagnetic low-spin state of Fe^{2+} ions in these species. Compounds **8** and **9**, with $[Zn(bpy)_3]^{2+}$ cation, should be diamagnetic and therefore, their magnetic properties were not examined at all. The data obtained for compounds **3**–**7** are given in Fig. 7, as the χT *vs.* T plot. It is evident that the compounds containing Ni^{2+} ions, *i.e.* **5** and **6**, show very similar and paramagnetic Curie behaviour almost to the lowest temperatures (the χT values are parallel to the T axis down to ~ 8 K), whereas compound **7**, with Cu^{2+}, retains this paramagnetic behaviour in the whole range of temperatures (*i.e.* down to 1.8 K). The χT values of ~ 0.42 and ~ 1.17 $cm^3mol^{-1}K$ (Fig. 7) for the Cu^{2+} and Ni^{2+} compounds, respectively, are consistent with the Curie expression:

$$\chi T = \frac{N_A \mu_B^2 g^2}{3k} S(S+1) \qquad (1)$$

where S = 1 and g = 2.16 for **5** and **6**, and S = 1/2 and g = 2.11 for **7**. A decrease of the χT product at temperatures below ~ 8 K, observed for compounds **5** and **6** is probably the

consequence of the zero-field splitting. Namely, the trigonal distortion of the ligand field and spin-orbit coupling (two perturbations of the second order) split the three spin components of the $^3A_2$ ground state of the octahedral Ni^{2+} ion.[3] The spin components $|-1\rangle$ and $|1\rangle$ have different ground state energy (D) from that of the spin component $|0\rangle$ (zero). The magnetic susceptibility in the direction of the trigonal distortion (χ_z) is different from that in the direction perpendicular to this distortion (χ_x):[3]

$$\chi_z = \frac{2N_A g^2 \beta^2}{kT} \frac{e^{-D/kT}}{1+2e^{-D/kT}} \tag{2}$$

$$\chi_x = \frac{2N_A g^2 \beta^2}{D} \frac{1-e^{-D/kT}}{1+2e^{-D/kT}} \tag{3}$$

The susceptibility of the pulverized samples (used in the measurements) is:

$$\chi = (\chi_z + 2\chi_x)/3 \tag{4}$$

The nonlinear fit procedure of the χT quantity [where χ is obtained from the equations (2)–(4)] on the experimental data leads to the following best fit parameters: $g = 2.1656(3)$, $D = 1.313(9)$ cm^{-1} and $g = 2.1540(2)$, $D = -1.449(9)$ cm^{-1} for **5** and **6**, respectively [with the discrepancy factors $R = \sum[(\chi T)_{obs} - (\chi T)_{calc}]^2 / \sum(\chi T)^2_{obs}$ equal to $3.30 \cdot 10^{-6}$ and $1.62 \cdot 10^{-6}$ for **5** and **6**, respectively]. The best fit curves are also shown in Fig. 7 as full lines – they match the measured data very well and correctly reproduce the decrease of the χT values at the lowest temperatures. The strait line passing through the measured data for the Cu^{2+} compound (**7**) is the best fit curve of the Curie model (1) with the best fit parameter $g = 2.1106(2)$ and with the R factor of $4.57 \cdot 10^{-6}$. Due to the Kramers theorem, the zero-field splitting is not possible for the Cu^{2+} ions (not even in distorted ligand field environments),[3] corroborating the observation evident from Fig. 7, *i.e.* the paramagnetic Curie behaviour within the whole temperature range of measurements.

The experimental data for the Co^{2+} compounds (**3** and **4**) show an increase of the χT values from ~ 1.65 cm^{3}mol^{-1}K at low temperatures to ~ 2.8 cm^{3}mol^{-1}K at room temperature. Such a behaviour is typical for the high-spin octahedral Co^{2+} complexes. The existence of the high-spin Co^{2+} ions is in accord with the Co−N bond lengths found in the crystal structures (see "Molecular structures and distortions of $[M(bpy)_3]^{2+}$ cations"). The obtained χT values above 30 K are greater than 1.88 cm^{3}mol^{-1}K, which is the value expected from the spin-only contribution of the high-spin Co^{2+} ion (S = 3/2) in the Curie law (1). This is an evidence of the orbital momentum contribution in the ground state of the octahedral Co^{2+} ion ($^4T_{1g}$). It is well

known that magnetic susceptibilities of the ions possessing first-order orbital momentum contribution significantly deviate from the Curie law, producing variations in the χT *vs. T* curve similar to that observed for compounds **3** and **4**.[3–7] In the present work, the susceptibility has been calculated according to the recent approach of Sakiyama,[42] wherein the six lowest $E_n^{(0)}$ energy states [and their first and second Zeeman $E_{n,z(x)}^{(1)}$ and $E_{n,z(x)}^{(2)}$ coefficients] are obtained from the Hamiltonian describing the high-spin Co^{2+} ion in the axially distorted ligand field environment:[3]

$$\hat{H} = \Delta\left(\hat{\mathbf{L}}_z^2 - 2/3\right) - (3/2)\kappa\lambda\hat{\mathbf{L}}\cdot\hat{\mathbf{S}} + \beta\left[-(3/2)\kappa\hat{\mathbf{L}} + g_e\hat{\mathbf{S}}\right]H \qquad (5)$$

In the above expression g_e is a *g*-value for the free electron (2.0023), λ is the spin-orbit coupling constant and Δ is the axial splitting parameter. The orbital reduction factor κ takes into account the covalency of the Co−N bonds and the admixture of the $^4T_{1g}(^4P)$ excited state into the $^4T_{1g}$ ground state,[3] whereas Δ is taken to be positive when the $^4A_2$ state is lower than the ^4E state (the states arising from the splitting of the octahedral $^4T_{1g}$ state under an axial ligand field distortion). Magnetic susceptibilities for the two specific directions in space (*z*, parallel with the axis of the ligand-field distortion and *x*, perpendicular to this axis) are obtained from the Van-Vleck equation:

$$\chi_{z(x)} = N_A \frac{\sum_n \left(\frac{E_{z(x),n}^{(1)\,2}}{kT} - 2E_{z(x),n}^{(2)} \right) \mathrm{Exp}\left[-\frac{E_n^{(0)}}{kT} \right]}{\sum_n \mathrm{Exp}\left[-\frac{E_n^{(0)}}{kT} \right]} \qquad (6)$$

whereas the susceptibility of pulverized samples is obtained from the averaging equation (4). Within this model, the nonlinear fit procedure of the χT quantity on the measured data leads to the following best fit parameters: $\Delta = 474(8)$ cm^{-1}, $\kappa = 0.800(2)$, $\lambda = -150.5(9)$ and $\Delta = 638(12)$ cm^{-1}, $\kappa = 0.826(3)$, $\lambda = -166(1)$ cm^{-1}, with the R factors equal to $1.24\cdot10^{-5}$ and $1.45\cdot10^{-5}$ for **3** and **4**, respectively. The best fit curves shown in Fig. 7 correspond very well to the experimental data for compounds **3** and **4**.

In the above theoretical models of magnetic susceptibilities (adjusted according to the appropriate ions) the ligand-field distortions were taken into account. The crystal structure analysis revealed the existence of these distortions (see "Molecular structures and distortions of $[M(bpy)_3]^{2+}$ cations"), which justifies their application in the given magnetochemical analysis. A very good correspondence of the applied models with the measured data shows that further refinements, like inclusion of the magnetic exchange interactions, are not necessary.

Conclusions

From the presented research of structural and magnetic properties of the novel complex salts $[M(bpy)_3]_2[NbO(C_2O_4)_3]Cl{\cdot}nH_2O$ [M = Fe^{2+}, Co^{2+}, Ni^{2+}, Cu^{2+} and Zn^{2+}; bpy = 2,2'-bipyridine; n = 11 (monoclinic form), 12 (orthorhombic form)] the following conclusions can be stressed: (i) in both types of structural forms $[M(bpy)_3]^{2+}$ cations are arranged in the honeycomb pseudo-hexagonal lattices formed by the QAE contacts, which can not be described in the terms of C−H$\cdots\pi$ or stacking interactions. The QAE contacts tend to preserve parallel orientation of molecular three-fold rotation axes and chiralities of the aggregated $[M(bpy)_3]^{2+}$ cations; (ii) the monoclinic and orthorhombic structural forms have different structures of hydrogen bonding layers emerging in both forms as the layers dividing honeycomb lattices of $[M(bpy)_3]^{2+}$ cations; (iii) the magnetic susceptibility measurements confirm that the new compounds are magnetically well diluted systems.[43] The reliable explanation of the magnetic measurements includes the axial distortions of the ligand fields. The observation that all molecular three-fold rotation axes of $[M(bpy)_3]^{2+}$ cations tend to be oriented in the *c** direction for both crystallographic forms (as a consequence of the QAE contacts) could make these compounds interesting in the research of magnetic anisotropies around the individual magnetic centres.

Acknowledgements

This research was supported by the Ministry of Science, Educations and Sports of the Republic of Croatia (Grants Nos. 098-0982904-2946, 119-1191458-1017, 119-1193079-3069).

References

1 C. B. Aakeröy, *Acta Crystallogr., Sect. B*, 1997, **53**, 569–586.

2 G. R. Desiraju, *Crystal Engineering: The Design of Organic Solids*, Elsevier, Amsterdam, 1989.

3 O. Kahn, *Molecular Magnetism*, Wiley-VCH, New York, 1993.

4 B. N. Figgis, *Trans. Faraday Soc.*, 1961, **57**, 198–203.

5 B. N. Figgis, J. Lewis, F. E. Mabbs and G. A. Webb, *J. Chem. Soc. A*, 1966, 1411–1421.

6 B. N. Figgis, J. Lewis, F. E. Mabbs and G. A. Webb, *J. Chem. Soc. A*, 1967, 442–447.

7 B. N. Figgis, M. Gerloch, J. Lewis, F. E. Mabbs and G. A. Webb, *J. Chem. Soc. A*, 1968, 2086–2093.

8 M. Gerloch, J. Lewis, G. G. Phillips and P. N. Quested, *J. Chem. Soc. A*, 1970, 1941–1955.

9 M. Gerloch and P. N. Quested, *J. Chem. Soc. A*, 1971, 3729–3741.

10 (a) U. García-Couceiro, O. Castillo, A. Luque, J. P. García-Terán, G. Beobide and P. Román, *Eur. J. Inorg. Chem.*, 2005, 4280–4290; (b) C. N. R. Rao, S. Natarajan and R. Vaidhyanathan, *Angew. Chem. Int. Ed.*, 2004, **43,** 1466–1496; (c) J.-H. Yu, Q. Hou, M.-H. Bi, Z.-L. Lü, X. Zhang, X.-J. Qu, J. Lu and J.-Q. Xu, *J. Mol. Struct.*, 2006, **800**, 69–73; (d) S. Triki, F. Bérézovsky, J. S. Pala, E. Coronado, C. J. Gómez-García, J. M. Clemente, A. Riou and P. Molinié, *Inorg. Chem.*, 2000, **39,** 3771–3776; (e) E. Coronado, J. R. Galán-Mascarós, C. J. Gómez-García, E. Martínez-Ferrero, M. Almeida and J. C. Waerenborgh, *Eur. J. Inorg. Chem.*, 2005, 2064–2070; (f) M. Gruselle, C. Train, K. Boubekeur, P. Gredin and N. Ovanesyan, *Coord. Chem. Rev.*, 2006, **250,** 2491–2500; (g) E. Coronado, J. R. Galán-Mascarós and C. Martí-Gastaldo, *J. Mater. Chem.*, 2006, **16** 2685–2689.

11 M. Jurić, B. Perić, N. Brničević, P. Planinić, D. Pajić, K. Zadro and G. Giester, *Polyhedron*, 2007, **26**, 659–672.

12 M. Jurić, P. Planinić, N. Brničević, D. Milić, D. Matković-Čalogović, D. Pajić and K. Zadro, *Eur. J. Inorg. Chem.*, 2006, 2701–2710.

13 (a) I. Dance and M. Scudder, *J. Chem. Soc., Dalton Trans.*, 1998, 1341–1350; (b) I. Dance, *CrystEngComm*, 2003, **5**, 208–221.

14 M. Šestan, B. Perić, G. Giester, P. Planinić and N. Brničević, *Struct. Chem.*, 2005, **16**, 409–414.

15 G. Mathern and R. Weiss, *Acta Crystallogr., Sect. B*, 1971, **27**, 1610–1618.

16 F. M. Jaeger and J. A. van Dijk, *Z. Anorg. Allg. Chem.*, 1936, **227**, 273–327.

17 M. Šestan, G. Giester and B. Perić, *Acta Crystallogr., Sect. C*, 2004, **C60**, 595–597.

18 P. W. Selwood, *Magnetochemistry*, Interscience Publishers, Inc., New York, 2nd edn., 1956.

19 Wolfram Research, Inc., *Mathematica* (Version 5.0), Champaign, USA, 2003.

20 Z. Otwinowski and W. Minor, *Methods in Enzymology*, vol. 276: *Macromolecular Crystallography*, part A, ed. C. W. Carter and R. M. Sweet, Academic Press, London, 1997, pp. 307–326.

21 Stoe & Cie, *STADI4* (Version 1.05b), *Diffractometer Control for Windows*, Darmstadt, Germany, 1995.

22 Stoe & Cie, *X-RED* (Version 1.05), *Data Reduction Program for Windows*, Darmstadt, Germany, 1995.

23 Bruker Nonius BV, *KappaCCD user manual, Revision 1.10*, Delfts, Netherlands, 1998.

24 G. M. Sheldrick, SHELXS-97, *Program for Crystal Structures Solution*, University of Göttingen, Germany, 1997.

25 G. M. Sheldrick, SHELXL-97, *Program for Crystal Structures Refinement*, University of Göttingen, Germany, 1997.

26 M. Nardelli, *J. Appl. Crystallogr*., 1999, **32**, 563–571.

27 L. J. Farrugia, *J. Appl. Crystallogr.*,1999, **32**, 837–838.

28 H. D. Flack, *Acta Crystallogr., Sect. A*, 1983, **39**, 876-881.

29 L. J. Farrugia, *J. Appl. Crystallogr.*, 1997, **30**, 568.

30 N. E. Brese and M. O'Keeffe, *Acta Crystallogr., Sect. B*, 1991, **47**, 192–197.

31 R. M. K. Deng, S. Simon, K. B. Dillon and A. E. Goeta, *Acta Crystallogr., Sect. C*, 2001, **57**, 4–6.

32 E. König, *Prog. Inorg. Chem.*, 1987, **35**, 527–622.

33 C. Ruiz-Pérez, P. A. L. Luis, F. Lloret and M. Julve, *Inorg. Chim. Acta*, 2002, **336,** 131–136.

34 E. I. Steifel and G. F. Brown, *Inorg. Chem.*, 1972, **11**, 434–436.

35 H. L. Schläfer and G. Gleimann, *Basic Principles of Ligand Field Theory*, Willey-Interscience, London, 1969.

36 F. A. Cotton, *Chemical Applications of Group Theory*, John Wiley & Sons, New York, 1990.

37 C. P. Brock and J. D. Dunitz, *Chem. Mater.*, 1994, **6**, 1118–1127.

38 S. Das, S. A. Maloor, Sat. Pal and Sam. Pal, *Cryst. Growth Des.*, 2006, **6**, 2103–2108.

39 L. Fábián and A. Kálmán, *Acta Crystallogr., Sect. B*, 1999, **55**, 1099–1108.

40 A. Kálmán, L. Párkányi and G. Argay, *Acta Crystallogr., Sect. B*, 1993, **49**, 1039–1049.

41 F. H. Allen, *Acta Crystallogr., Sect. B*, 2002, **58**, 380–388.

42 H. Sakiyama, R. Ito, H. Kumagai, K. Inoue, M. Sakamoto, Y. Nishida and M. Yamasaki, *Eur. J. Inorg. Chem.*, 2001, **8**, 2027–2032.

43 S. Hatscher, H. Schilder, H. Lueken and W. Urland, *Pure Appl. Chem*. 2005, **77**, 497–511.

Figure captions

Fig. 1. ORTEP-3[29] drawings of: (a) the **A** and **B** cations of the orthorhombic compound **2**, (b) the **A** and **B** cations of the monoclinic compound **8**, (c) $[NbO(C_2O_4)_3]^{3-}$ anion (compound **2**), with the atomic numbering schemes.

Fig. 2. (a) Nitrogen atoms around metal (M) atom defining the intertriangle distance *h* and the triangle side *s* for the calculation of the compression ratio *s*/*h*.[34]
(b) View of the octahedron of nitrogen atoms along the C_3 axis illustrating the twisting angle ϕ.[34]

Fig. 3. Stereoviews of crystal packing in the orthorhombic (a) and monoclinic (b) structures. Hydrogen atoms are omitted for the reason of clarity.

Fig. 4. Crystal packing of $[M(bpy)_3]^{2+}$ cations in the orthorhombic compounds (**2**, **4**, **6** and **7**) realized by three symmetry independent types of the QAE contacts. The symmetry codes and bpy ligands involved in the contacts are labelled according to Table 3 and Fig. 1a.

Fig. 5. Crystal packing of $[M(bpy)_3]^{2+}$ cations in the monoclinic compounds (**3**, **5** and **8**) realized by three symmetry independent types of the QAE contacts. The symmetry codes and bpy ligands involved in the contacts are labelled according to Table 3 and Fig. 1b.

Fig. 6. Two-dimensional hydrogen bonding layers in the structures are connected by one [(a), orthorhombic form] or two [(b), monoclinic form] crystal water molecules.

Fig. 7. Temperature dependence of χT for compounds **3**–**7**. The solid lines represent the curves of the best fit in the model of axially distorted ligand field.

Graphical and textual abstract for the contents pages

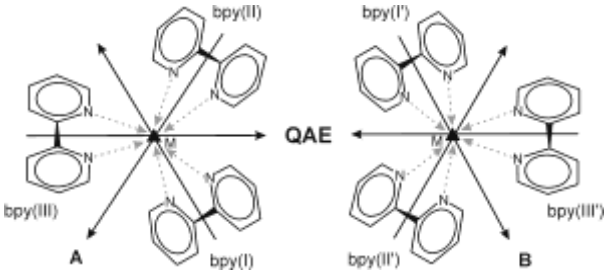

Two isostructural sets of solvatomorphs, $[M(bpy)_3]_2[NbO(C_2O_4)_3]Cl\cdot nH_2O$, crystallizing in the $P2_1/c$ (n = 11) or $P2_12_12_1$ (n = 12) space groups have been characterized by spectroscopic, X-ray structural and magnetic-susceptibility measurements. A specific supramolecular contact, comprising four bipyridine ligands from two neighbouring $[M(bpy)_3]^{2+}$ cations has been identified and described.